EurJIC
European Journal of Inorganic Chemistry

Full Papers
doi.org/10.1002/ejic.202100580

Chemistry Europe
European Chemical Societies Publishing

Coordination Chemistry and Sensing Properties Towards Anions and Metal Ions of a Simple Fluorescent Urea

Riccardo Montis,[a] M. Carla Aragoni,[b] Massimiliano Arca,[b] Simon J. Coles,[c] Vito Lippolis,[b] Jessica Milia,[b] James B. Orton,[c] Laura Pala,[b] Giacomo Picci,*[b] Tiziana Pivetta,[b] and Claudia Caltagirone*[b]

The coordination and sensing properties towards anions and transition metal ions of the simple novel fluorescent urea 1-(2-aminophenyl)-3-(naphthalen-1-yl)urea (**L**) were investigated in solution, and in the solid state. An electron donating amine group in the molecular skeleton of **L** decreased the acidity of the urea NHs that are usually deprotonated by basic anions and allowed for a good degree of affinity towards fluoride in DMSO-d_6-0.5 %H_2O. Moreover, the amine moiety acted as a further binding group for metal ions. Indeed, **L** was able to bind Zn^{2+} both in solution and in the solid state, and to respond to the presence of this metal ion in MeCN with an enhancement of the fluorescence emission. Although solution studies evidenced the formation of a 1:1 complex of **L** with Zn^{2+}, complexes with a 2:1 ligand-to-metal stoichiometry were isolated in the solid state. DFT calculations helped to clarify the stability reasons behind these results.

Introduction

Urea was landmark molecule during the development of modern organic chemistry. Indeed, prior to its first synthesis by Wohler in 1828,[1] it was believed that the synthesis of organic molecules could only pertain to living organisms. Since then, urea assumed a pivotal role in chemistry for its use as fertilizer, as raw chemical for the synthesis of urea-formaldehyde resins, as an additive to decrease the emission of NO_x in industry, in the synthesis of drugs, such as barbiturates or anti-cancer drugs.[2] Recently, urea has become a fundamental synthon in supramolecular chemistry used for the development of functional materials such as capsules, gels, and polymers.[3] Its versatility arises from multiple factors. In particular, it can act as an efficient hydrogen bond donor (due to the presence of the NH groups), a feature exploited in the development of receptors able to selectively bind, recognize (sense) and transport anions. Indeed, a high number of urea-based (and also thiourea and selenourea) receptors have been developed during the last 30 years for these purposes.[4,5] The planarity of the urea moiety allows for the two NHs group to be parallel, and thus perfectly oriented to coordinate carbonyl groups. This makes urea-containing receptors particularly suitable for carboxylates binding,[6] but also appealing components for catalysis applications since the pioneering work by Etter and Panunto at the end of the '80s.[7] On the other hand, due to the presence carbonyl group, urea can be used also to bind metal ions as a monodentate ligand, while the N, O bidentate coordination mode is less common.[8] It is worth noting that the active site of the urease enzyme features a dinuclear Ni(II) cluster that interacts with the urea substrate acting as N, O bridging ligands.[9] Some of the authors have recently reported on the coordination properties of a new derivative of [9] ane N_3 (1,4,7-triazacyclononane) bearing three phenyl pendant arms and ureas as functional group spacers.[10] In particular, a rare example of a copper (II) complex with this ligand was prepared, in which one of the coordination sites of the octahedral metal coordination sphere was occupied by a nitrogen atom of one of the phenyl urea pendant arms. Other examples of metal coordination by urea-containing ligands were reported by Esteban-Gomez and co-workers.[11] Following our interest in the development of new systems able to bind anions and to sense metal ions, we report here the binding affinity and coordination properties towards anions and metal ions of a simple fluorescent phenylurea receptor (**L**, Scheme 1) bearing a naphthyl group as a fluorogenic unit on one side and an amino group in *ortho* position of a phenyl ring on the other side. The amino group was introduced with a dual purpose: its electron-donating nature is expected to decrease the acidity of the urea NHs, thus allowing for the binding of basic anions such as fluoride;[12,13] its coordination properties could supplement metal ions binding.

[a] *Dr. R. Montis*
Università degli Studi di Urbino Carlo Bo,
Dipartimento di Scienze Pure e Applicate,
Laboratorio di Chimica Supramolecolare
Via della Stazione 4, 61029 Urbino, Italy
[b] *Prof. M. C. Aragoni, Prof. M. Arca, Prof. V. Lippolis, J. Milia, Dr. L. Pala, Dr. G. Picci, Prof. T. Pivetta, Prof. C. Caltagirone*
Università degli Studi di Cagliari, Dipartimento di Scienze Chimiche e Geologiche
Bivio per Sestu S. S. 554, 09042 Monserrato (CA), Italy
E-mail: gpicci@unica.it
ccaltagirone@unica.it
[c] *Prof. S. J. Coles, Dr. J. B. Orton*
Chemistry University of Southampton
Highfield, Southampton SO17 1BJ, UK

Supporting information for this article is available on the WWW under https://doi.org/10.1002/ejic.202100580

Part of the "44th ICCC Conference" Special Collection.

Full Papers
doi.org/10.1002/ejic.202100580

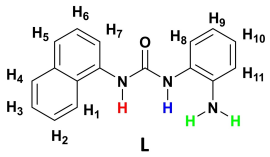

Scheme 1. Receptor **L** with the colour and numbering scheme adopted in the 1H-NMR studies discussion.

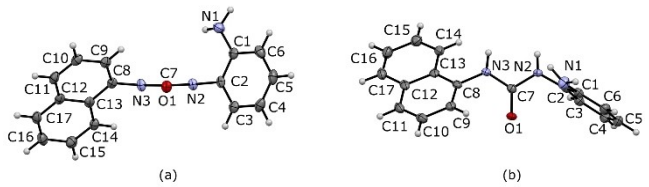

Figure 1. Ortep views and numbering scheme of **L** determined by scXRD (ellipsoids probability level: 50%), viewed down two perpendicular directions. For bond lengths and angles and for torsion angles see Tables S2–S4 in SI.

Results and Discussion

Synthesis and characterization of L

The synthesis of 1-(2-aminophenyl)-3-(naphthalen-1-yl)urea (**L**) was performed by reacting the *o*-phenylendiamine with the 1-naphthylisocyanate in dichloromethane (DCM) under N_2 atmosphere. The desired product was collected as a white solid in 95% yield (see Supporting Information, SI, Figures S1–S3 for ^{1}H, ^{13}C, and ESI mass spectra of **L**). Crystals of the free receptor **L** suitable for single crystal X-ray diffraction (scXRD) analysis were obtained by slow evaporation of a solution of **L** in DMSO. **L** crystallized in the orthorhombic crystal system (space group $P2_12_12_1$, see also SI, Table S1, and Tables S2–S4 for selected bond distances and angles). The asymmetric unit consists of one **L** molecule ($Z' = 1$), with the aminophenyl and the naphthyl moieties tilted with respect the plane of the urea moiety (C1-C2-N2-C7 and C9-C8-N3-C7 torsion angles are −95.1(3)° and 46.0(3)° respectively), resulting in a non-planar conformer (Figure 1). An almost identical conformation was previously observed in 1-(2-aminophenyl)-3-phenylurea.[14]

Units of **L** are connected to adjacent molecules by N–H···O hydrogen bonds (H···O distances are 2.22(3) and 1.97(3) Å), forming 1-D urea chains running along the a direction (see SI, Figure S4 and Table S5), a robust and common supramolecular arrangement in crystal structures of urea derivatives.[14–15] The 1-D urea chains are then packed along the remaining two dimensions, interacting *via* sets of N–H···O, N–H···N hydrogen bonds (H···O and H···N distances are 2.18(3) and 2.15(2) respectively), involving the urea C=O, and the NH_2 functional groups (see SI, Figure S4).

Anion binding studies in solution

In order to evaluate the anion binding affinity of **L**, ^{1}H-NMR titrations in DMSO-d_6-0.5% H_2O as a solvent were performed with fluoride (F^-), acetate (AcO^-) benzoate (BzO^-), hydroxide (OH^-) and dihydrogen phosphate ($H_2PO_4^-$) as their tetrabutylammonium salts. Stability constants from the obtained ^{1}H-NMR titration curves (see Supporting Information, Figures S5–S8) were calculated by fitting the data with a 1:1 binding model using Bindifit[16] as shown in Table 1.

Table 1. Association constants (K_s/M^{-1}) for the formation of 1:1 adducts of **L** with anions added as tetrabutylammonium salts in DMSO-d_6-0.5% H_2O at 298 K obtained by following the downfield shift of the signals attributed to the urea NHs and to the amine NH_2. All errors estimated to be ≤20.0%.

	F^-	AcO^-	BzO^-	$H_2PO_4^-$
L	953	630	243	631[a]

[a] The signal attributed to the amine group disappeared upon addition of 0.2 equivs of $H_2PO_4^-$.

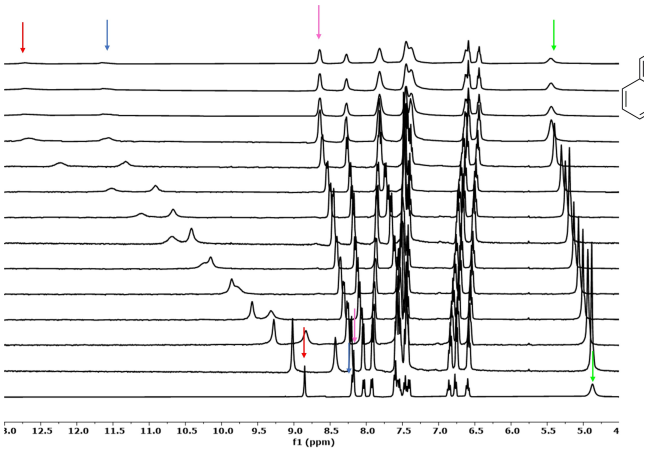

Figure 2. Stack-plot of the ^{1}H-NMR titration in DMSO-d_6-0.5% H_2O at 298 K of **L** (0.005 M) with fluoride added as tetrabutylammonium salt (0.075 M).

The data reported in Table 1 shows that the highest stability constant was obtained for the formation of the 1:1 adduct of **L** with F^-. As shown in the stack plot reported in Figure 2 the 1:1 adduct with fluoride is formed in solution *via* the formation of three H-bonds (two with the urea NHs, singlet signals at 8.85 and 8.20 ppm, red and blue, respectively, and one with the amine NH_2, singlet signal at 4.85 ppm, green) and another, presumably weaker, interaction with the CH adjacent to the amine NH_2 (doublet signal at 8.18 ppm, magenta labelled as H11 in Scheme 1).

In the case of $H_2PO_4^-$ the disappearance of the signal attributed to the singlet at 4.85 ppm (probably in exchange with the water present in solution) attributed to the NH_2 group allowed us only to follow the downfield shift of the two urea NHs and the naphthyl CH (SI, Figure S8).

As expected, the presence of the electron donating amino group in the backbone of the receptor prevented the deprotonation of the urea NHs by fluoride otherwise observed in N,N′-diphenylurea derivatives.[15a] A detailed study of fluoride binding both in solution and in the solid state with ureas, amides and squaramides was reported by Gouverneur and coworkers.[17] The

formation of the adduct between TBAAcO and analogous receptor 1-naphtalen-1yl-3-phenyl-urea was studied by Leito and co-workers and a stability constant of 525 was determined suggesting that the presence of the amine group on **L** that could take part to the anion binding, slightly improves the affinity towards acetate.[6a] In the case of 1-naphthalen-1-yl-3-(2-nitro-phenyl)-urea, as expected, fluoride caused a deprotonation of the receptor.[18]

An immediate disappearence of the signals attributed to the urea NHs was observed upon the addition of 0.1 eqvs. of TBAOH accompanied by a colour change of the solution form colourless to yellow. The colour of the solution gradually became more intense untill, in the presence of 1.5 eqvs. of TBAOH, turned red, as a consequence of the deprotonation of the amine group (see SI Figure S6).

Spectrophotometric and spectrofluorimetric titrations were conducted with the same set of anions both in DMSO-0.5% H_2O and in MeCN to test the different response of **L** by varying the polarity of the medium. In both solvents (DMSO-0.5% H_2O and in MeCN) **L** shows an absorption band at around 312 nm and 298 nm, respectively ($\varepsilon_{DMSO} = 11800\ M^{-1}cm^{-1}$, $\varepsilon_{MeCN} = 12700\ M^{-1}cm^{-1}$). An emission band centered at 374 nm ($\lambda_{exc} = 300$ nm) and 367 nm ($\lambda_{exc} = 285$ nm) was observed in DMSO-0.5% H_2O and MeCN solutions, respectively (SI, Figure S9). In MeCN the addition of increasing amounts of the set of anions considered to a solution of **L** caused a bathochromic shift of the absorption band of the free receptor (SI, Figure S10) with the formation of two isosbestic points (ranging between 270–273 nm and 297–300 nm) and a complete quenching of the fluorescence emission (Figure 3). A similar quenching was observed in analogous systems.[18]

In DMSO the changes in the UV-Vis spectra were negligible (SI, Figure S11), while the quenching of the fluorescence was less dramatic (SI, Figure S12) with all the anions studied. This behavior can be possibly attributed to the different competition effects of the two solvents that allows an increase of the affinity towards anions of **L** in MeCN.

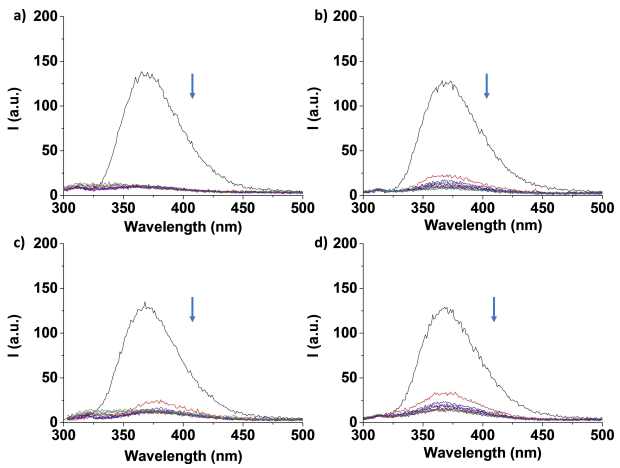

Figure 3. Fluorescence titrations of **L** ($2.5 \cdot 10^{-5}$ M) in MeCN with a) AcO^-, b) BzO^-, c) F^-, d) $H_2PO_4^-$.

Metal ion binding in solution and solid-state studies

The affinity of **L** for metal ions was also tested.

A preliminary screening of the coordination properties of **L** towards a set of transition metal ions, such as Zn^{2+}, Cu^{2+}, Cd^{2+}, Hg^{2+}, Pb^{2+}, Co^{2+}, Mn^{2+}, Ni^{2+} as their nitrate or perchlorate salts, was conducted in MeCN. No changes were observed in the case of Cd^{2+}, Pb^{2+}, Co^{2+}, and Ni^{2+} (SI, Figure S13), while Zn^{2+} (Figure 4a), Hg^{2+} and Mn^{2+} (SI, Figure S13c, S13d, respectively) caused a decrease and a hypsochromic shift of the absorption band of the free receptor, suggesting an interaction between **L** and these metal ions. Interestingly, among all metal ions considered, only Zn^{2+} caused an increase in the emission of **L** (Figure 4b) as a consequence of the formation of a 1:1 complex (Figure 4c). The stoichiometry of the complex was confirmed by a Job plot analysis (Figure 4d). A stability constant of $K_a = 60200\ M^{-1}$ was calculated by fitting the data of the UV-Vis titration with a 1:1 binding model using the open source software BindFit[16] (see SI).

ESI mass spectrometry further demonstrated that the 1:1 complex is the predominant species in solution. In the ESI (+) mass spectrum of a MeCN solution of a 2:1 mixture of **L** and $Zn(ClO_4)_2\ 6H_2O$, a peak at 717 *m/z* and a peak at 481 *m/z*, due to the species $[(Zn\mathbf{L}_2(ClO_4)]^+$ and $[Zn\mathbf{L}(ClO_4)(CH_3CN)]^+$, respectively, were observed (about 1 to 7 relative abundance, Figure S14). Precursor ion and parent fragmentation scan experiments revealed that the species $[Zn\mathbf{L}(ClO_4)(CH_3CN)]^+$ was not originated by $[Zn\mathbf{L}_2(ClO_4)]^+$ fragmentation, but it is the predominant species in solution. The complex stoichiometry assignment was based on the fitting of the isotopic pattern. All the masses were given considering the most abundant peak.

In order to further investigate the behavior of **L** in the presence of the Zn^{2+}, ^{1}H-NMR titrations in CD_3CN as a solvent were performed. All the protons were assigned according to 2D-NMR experiments (see SI Figure S15a and Figure S15b).

As shown in Figure 5, upon the addition of increasing amounts of Zn^{2+} (as perchlorate salt hydrate), the downfield shift of the

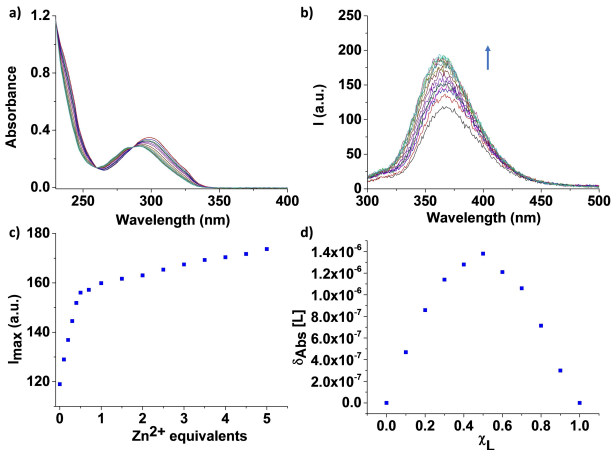

Figure 4. a) UV-Vis and b) fluorescence titration of **L** ($2.5 \cdot 10^{-5}$ M) in MeCN with $Zn(ClO_4)_2\ 6H_2O$ ($2.5 \cdot 10^{-3}$ M), $\lambda_{exc} = 285$ nm, c) plot of fluorescence I_{max} *vs* added Zn^{2+} equivalents for the fluorescence titration of **L** ($2.5 \cdot 10^{-5}$ M) in MeCN with $Zn(ClO_4)_2\ 6H_2O$, $\lambda_{max} = 367$ nm, d) Job plot of **L** and Zn^{2+} suggesting the formation of a 1:1 complex in MeCN.

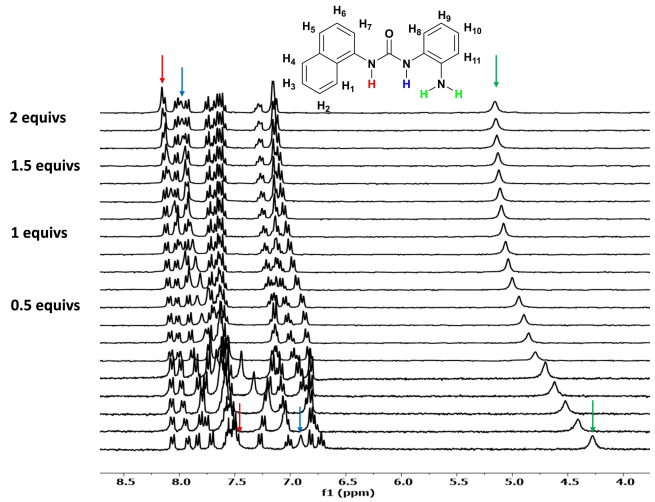

Figure 5. Stack-plot of the ^{1}H NMR titration of in CD_3CN of **L** (0.0025 M) in the presence of increasing amount of $Zn(ClO_4)_2$ $6H_2O$ (0.017 M).

signals attributed to the urea NHs at 7.52 ppm ($\Delta\delta = 0.63$ ppm) and 6.91 ppm ($\Delta\delta = 1.08$ ppm), indicated in red and blue, respectively, was observed, along with the downfield shift of the signal attributed to the amino group at 4.28 ppm ($\Delta\delta = 0.87$ ppm) indicated in green. This experimental evidence was likely due to the electronic rearrangement of the urea moiety of **L**, perhaps as a consequence of the involvement of the carbonyl group and the amino group in the metal ion coordination.

Furthermore, the chemical shift of all the signals attributed to the phenyl and the naphthyl moieties was observed. Particularly, the downfield shift of the signals attributed to the naphthyl moiety (labelled H_2-H_6 in Figure 1), and to the phenyl moiety (labelled H_8-H_{11} in Figure 1) was observed, accompanied by the shift to higher frequency of the signals attributed to the hydrogens H_1 and H_7 of the naphthyl moiety adjacent to the urea NH indicated in red. These observations further suggested that the electronic rearrangement of the urea moiety of **L** involved both the electronic spheres of the aromatic substituents. This behavior might explain the enhancement of the emission band observed in the fluorescence titrations conducted in this medium.

Various attempts to isolate the metal complexes of **L** with different metal ions were performed. Crystals suitable for single crystal X-ray diffraction analysis were only obtained in the case of Zn^{2+}. Namely, the two compounds $[Zn(\mathbf{L})_2(MeCN)_2](ClO_4)_2 \cdot 2MeCN$ (**1**) and $[Zn(\mathbf{L})_2(MeCN)_2](BF_4)_2 \cdot 2MeCN$ (**2**) were both isolated by slow diffusion of diethyl ether vapors into a MeCN solution of **L**, in the presence of 1:1 stoichiometric ratios of $Zn(ClO_4)_2 \cdot 6H_2O$ and $Zn(BF_4)_2 \cdot xH_2O$, respectively (SI, Table S1).

In both cases, the reaction resulted in salts of a cation showing a 2:1 **L**:Zn^{2+} stoichiometry. This is not consistent with the results of the solution studies, which suggested the formation of 1:1 complexes. Considering the different stability of the 1:1 and 2:1 complex cations (see below) may explain the discrepancy between solution studies and products of crystallization.

Apart some difference in the crystal packing (see SI, Figure S16, Table S1, and Tables S2–S4 for selected bond distances and angles), the crystal structures of compounds **1** and **2** show very similar features and can be described together.

Both complexes crystallized in the monoclinic crystal system ($P2_1/n$). The asymmetric unit consists of one counterion (ClO_4^- or BF_4^-, for structure **1** and **2** respectively), one molecule of MeCN and a half molecule of the $[Zn(\mathbf{L})_2(MeCN)_2]^{2+}$ complex ($Z' = 0.5$), with the central coordinated Zn^{2+} lying on an inversion center. Differently to the structure of **1**, in the structure of **2**, the relative position of the counterion and the solvent molecule are exchanged (see Figure 6a and Figure 6b). The complexes adopt an octahedral geometry as the majority of the Zn^{2+}-urea structures reported in the literature (coordination angles are in the range 86.69(4)°–93.31(4)° for both structures), with the four equatorial positions occupied respectively by one urea function and one amino group from two molecules of **L**, resulting in a L:Zn^{2+} 2:1 stoichiometry. As one would expect,[19] the urea coordinates as a monodentate ligand through the carbonyl C=O oxygen. Only in rare cases urea ligands showed an unusual bidentate coordination, also involving one of the urea nitrogen atoms.[10,11,20] In both cases, the remaining two axial positions, are occupied by two molecules of MeCN. Only few crystal structures of Zn^{2+} complexes with urea containing receptors bearing additional coordinating groups have been reported in the literature. Interestingly, we observed that while in urea-hydrazide derivatives the metal center is coordinated both by the carbonyl group and the hydrazide NH_2,[21] in urea receptors substituted with pyridine groups, the metal ion is coordinated solely by the pyridine nitrogen without any involvement of the urea moiety.[22]

Similar to the case of the structure of the free receptor (Figure 1), in structures **1** and **2**, **L** adopts a non-planar conformation (Figure 6c), with the aminophenyl and the naphthyl moieties both slightly tilted with respect the plane of the urea function (C1-C2-N2-C7 and C9-C8-N3-C7 torsion angles are 59.36(19)° and 54.03(19)° for **1** and 55.7(3)° and 46.3(3)° for **2**) but

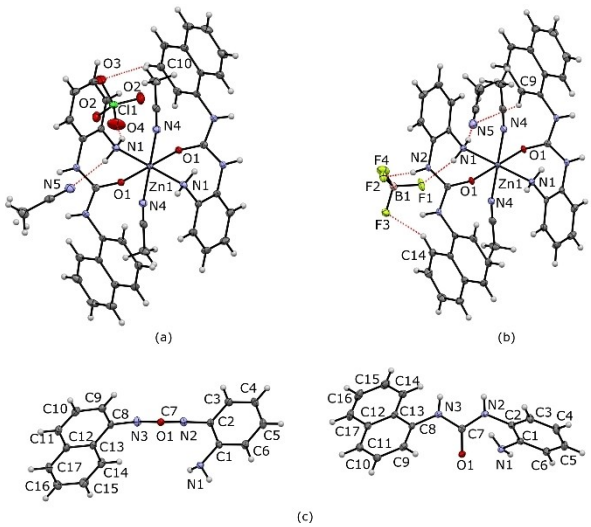

Figure 6. Ortep views of compounds (a) **1**, (b) **2** (ellipsoids probability level: 50%) as determined by scXRD; (c) conformation of **L**, shown for **1** as representative, viewed down two perpendicular directions. For bond lengths and angles and for torsion angles see Tables S2–S4 in SI.

with the amino group and the carbonyl oxygen oriented toward the same side of the molecule, allowing the coordination of the Zn^{2+} ion. This is consistent with the results from ^{1}H-NMR solution studies that suggested a coordination involving the amino group and the urea carbonyl donor. In both structures, the urea NH groups interact with the counterions via N–H···A (A = F or O) hydrogen bonds (see SI, Table S5) that bridge adjacent coordinated units along the three directions of the packing (see SI, Figure S16).

Theoretical calculations

DFT calculations were carried out in order to investigate the nature of the products formed when the ligand **L** is reacted with the Zn^{2+} ion (Tables S6–S14). The geometry of the ligand was optimized at DFT level (mPW1PW functional,[23] Def2SVP basis set[24] (Figure 7, Table S6).

The optimized metric parameters are in very good agreement with the corresponding ones determined by X-ray diffraction (see Tables S2-S4). Remarkable differences were found in the torsion angles of the aromatic substituents. The potential energy surfaces (PES) of the systems were therefore investigated as function of the rotation of the 2-aminophenyl and 2-naphthyl substituents. In both cases, only minor rotational barriers were found (3.85 and 7.76 kcal mol^{-1}, respectively; SI, Figure S17), so that the discrepancies reflect most likely crystal packing effects.

The Kohn-Sham (KS) HOMO of the ligand consists of the nitrogen lone pair of electrons (LP) localized on the amino substituent at the phenyl ring (natural charge −0.806 |e|),[25] while the LPs of the oxygen atom (natural charge −0.641 |e|)[25] contribute to the HOMO-4 and HOMO-5, and HOMO-6 SI, Figure S18).

DFT calculations on the complex cation $[Zn(\mathbf{L})_2(MeCN)_2]^{2+}$ show an excellent agreement between the calculated metric parameters (Table S7) and those determined by scXRD analysis on compounds **1** and **2** (Tables S2–4). Notably, the coordination environment at the central Zn^{2+} ion is described correctly at this level of theory (Zn–O, 2.063; Zn–NH_2, 2.162; Zn–NCMe, 2.208 Å; O–Zn–O, 179.99; N–Zn–N, 179.99°). Calculations were therefore extended to the 1:1 complex, identified in solution based on spectrophotometric data (see above).

Although no structural information on this complex is available, two possible coordination environments can be considered more likely in MeCN solution, *i.e.* $[Zn(\mathbf{L})(MeCN)_2]^{2+}$ and $[Zn(\mathbf{L})(MeCN)_4]^{2+}$ showing a tetrahedral and an octahedral coordination at the metal ion, respectively (Figure 8). Both complex cations were successfully optimized and verified by frequency calculations (Tables S8 and S9).

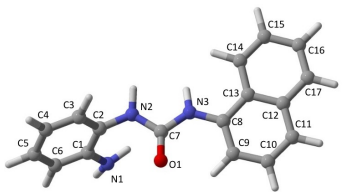

Figure 7. Representation of the ligand **L** at the DFT-optimized geometry in the gas phase. Selected bond distances and angles: C7-O1, 1.208; C7-N3, 1.384; C7-N2, 1.391, N3-C8, 1.398; N2-C2, 1.392 Å; N2-C7-N3, 111.85; C7-N3-C8, 128.17; C7-N2-C2, 121.23°; C1-C2-N2-C7, 102.35°; C9-C8-N3-C7, 9.40°.

Thermochemistry calculations (Table 2 and Table S15 and Table S16 in SI) were carried out in order to investigate the relative stabilities of 1:1 complexes $[Zn(\mathbf{L})(MeCN)_2]^{2+}$ and $[Zn(\mathbf{L})(MeCN)_4]^{2+}$ and the 1:2 complex $[Zn(\mathbf{L})_2(MeCN)_2]^{2+}$, isolated in the solid state. Therefore, the following model reactions were considered:

(i) $([Zn(\mathbf{L})_2(MeCN)_2]^{2+} \rightarrow [Zn(\mathbf{L})(MeCN)_2]^{2+} + \mathbf{L}$

(ii) $[Zn(\mathbf{L})_2(MeCN)_2]^{2+} + 2\ MeCN \rightarrow [Zn(\mathbf{L})(MeCN)_4]^{2+} + \mathbf{L}$

The sum of electronic and thermal free energies allows a direct comparison of the reaction Gibbs free energy ΔGr for reactions i) and ii) at 298.15 K, correspond to 143 and 43 kJ mol^{-1}, respectively (Table 2).

These values indicate that both reactions are endergonic both in the gas phase (Table S15 and Table S16) and in MeCN solution, taken into account at self-consistent reaction field (SCRF) level (Table 2), confirm the stability of the complex cation $[Zn(\mathbf{L})_2(MeCN)_2]^{2+}$, and suggest that the hexacoordinate complex $[Zn(\mathbf{L})(MeCN)_4]^{2+}$ would be less thermodynamically favored in MeCN solution as compared to the tetracoordinated $[Zn(\mathbf{L})(MeCN)_2]^{2+}$.

Thermochemical data suggest that the formation of the 1:2 metal-to-ligand complex would be thermodynamically favored over that of the 1:1 species. This notwithstanding the difference in the stability of the 1:2 and 1:1 (both tetra- and hexa-coordinated) complexes dramatically decreases on passing from

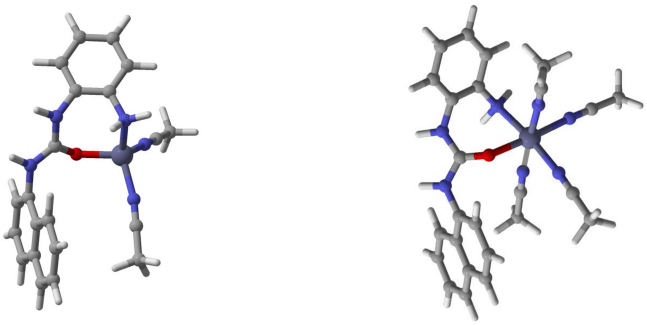

Figure 8. Molecular drawings of the model complexes $[Zn(\mathbf{L})(MeCN)_2]^{2+}$ (left) and $[Zn(\mathbf{L})(MeCN)_4]^{2+}$ (right).

Table 2. Calculated variations (kJ mol^{-1}) in total electronic energy ($\Delta\varepsilon_0$), enthalpy (ΔH_r) and free energy (ΔG_r) for the reactions involving $[Zn(\mathbf{L})_x(MeCN)_y]^{2+}$ complex cations in MeCN (x = 1, y = 2, 4; x = 2, y = 2) calculated in MeCN at IEF-PCM SCRF DFT level at 298.15 K.

	$\Delta\varepsilon_0$	ΔH_r	ΔG_r
$[Zn(\mathbf{L})_2(MeCN)_2]^{2+} \rightarrow [Zn(\mathbf{L})(MeCN)_2]^{2+} + \mathbf{L}$	85.0	73.9	15.9
$[Zn(\mathbf{L})_2(MeCN)_2]^{2+} + 2MeCN \rightarrow [Zn(\mathbf{L})(MeCN)_4]^{2+} + \mathbf{L}$	15.8	17.7	27.4
$[Zn(\mathbf{L})(MeCN)_2]^{2+} + 2MeCN \rightarrow [Zn(\mathbf{L})(MeCN)_4]^{2+}$	−69.2	−56.3	11.5

the gas-phase (Tables S15 and S16) to the MeCN solution (Table 2). This might suggest that the formation of the 1:1 complex would occur in solution under kinetic control, while the most stable 1:2 complex would be the most stable species under thermodynamic control. This is consistent with the fact that both crystallizations of **1** and **2** from a 1:1 reaction mixture, reproducibly gave the 2:1 complexes as the only products.

As regards the relative stabilities of the 1:1 species $[Zn(\mathbf{L})(MeCN)_2]^{2+}$ and $[Zn(\mathbf{L})(MeCN)_4]^{2+}$, the Gibbs free energy ΔG_r for the reaction:

$$\text{(iii)}\ \ [Zn(\mathbf{L})(MeCN)_2]^{2+} + 2\ MeCN \rightarrow [Zn(\mathbf{L})(MeCN)_4]^{2+}$$

is calculated to be as large as 11.5 kJ mol^{-1} in MeCN solution. Therefore, DFT calculations provide a suggestion of $[Zn(\mathbf{L})(MeCN)_2]^{2+}$ as the most likely complex cation showing a 1:1 Zn:**L** ratio (Table 2).

Finally, time-dependent DFT (TD-DFT) calculations were carried out for a better understanding of the optical properties of **L** and the relevant Zn complexes. The UV-Vis absorption at the lowest energy (from the ground state to the first singlet excited state, GS→ES1) is calculated in the gas phase at λ_{ES1} = 312.5 nm (E_{ES1} = 3.968 eV, oscillator strength f = 0.172) and is attributed to a monoelectronic excitation from the π-in-nature Kohn-Sham (KS) HOMO (localized on the phenyl portion of **L**) to the π-KS-LUMO (localized on the naphthyl moiety). Very similar values are calculated upon considering solvation (λ_{ES1} = 310.5 nm; E_{ES1} = 3.993 eV, f = 0.258 in MeCN; Figure S19 in SI). Notably, due to the frontier molecular orbital composition, the probability of the transition is strongly dependent on the mutual orientation of the two aromatic substituents, which is expected to vary in solution at room temperature due to the low rotational barrier discussed above. Due to the conformation assumed by **L** in the complex (Figure 8 left), in the complex cation $[Zn(\mathbf{L})(MeCN)_2]^{2+}$, the absorption at the lowest energy is calculated to involve π-MOs on the ligand **L** (λ_{ES1} = 288.5 nm; E_{ES1} = 4.297 eV, f = 0.202 in MeCN; Figure S20 in SI), entirely localized on the naphthyl portion of the ligand (see Figure S21 in SI). Notably, in agreement with the experimental data (see above), a hypsochromic shift (ΔE_{ES1} = 0.304 eV, resulting in $\Delta\lambda_{ES1}$ = 22 nm) is calculated with the corresponding band calculated under the same condition for the free ligand. At the geometry imposed by Zn^{II} coordination, the GS→ES1 excitation only involve MOs localized on the naphthyl substituent, strongly rotated with respect to the urea fragment (119.67°). Upon excitation, after a vibrational relaxation (internal conversion) from the upper excited states to ES1, the radiative emission ES1→GS would occur within the naphthyl pendant. This might tentatively explain the increase in the fluorescent emission of **L** in the presence of Zn^{II} ions.

Conclusion

In conclusion, the introduction of an amino group in the molecular skeleton of the simple urea receptor **L** was proved to offer different advantages. First, the electron donating properties of the amine moiety prevented the deprotonation of the urea NHs offering the possibility to bind basic anions such as fluoride. Indeed, the value of the stability constant measured by ^{1}H-NMR titrations in DMSO-d_6-0.5 %H_2O with fluoride was almost twice higher than that observed with the other anions studied. The formation of 1:1 anion adducts in solution was also confirmed by UV-Vis and fluorescence both in DMSO 0.5 % H_2O and in MeCN. Moreover, the presence of the amino group also offered a supplemental binding site for metal ions. In the solid state two complexes of **L** with Zn^{2+} were isolated In this case a selectivity in terms of fluorescence response towards Zn^{2+} was observed in MeCN solution due to the formation of the 1:1 complex. DFT calculations suggested that the formation of the 1:1 complex of **L** with Zn^{2+} is under kinetic control while the 2:1 stoichiometry observed in the solid state is the most stable- thermodynamically controlled- final product. Overall, this study confirms that urea is a fundamental synthon in the design of supramolecular systems able to bind both anions and metal ions. In particular, the introduction of supplemental functional groups on the urea skeleton able to modulate both the acidity of the urea NHs and able to act as donor groups for the coordination of metal ions, can improve the performances of urea-based molecular sensors. This design strategy has not been much explored so far.[12]

Experimental Section

All reactions were performed in oven-dried glassware under a slight positive pressure of nitrogen. ^{1}H-NMR (400 MHz) and ^{13}C NMR (100 MHz) spectra were determined on a Varian INOVA-400 spectrometer. Chemical shifts for ^{1}H-NMR are reported in parts per million (ppm), calibrated to the residual solvent peak set, with coupling constants reported in Hertz (Hz). The following abbreviations are used for spin multiplicity: s = singlet, d = doublet, t = triplet, m = multiplet. Chemical shifts for ^{13}C NMR are reported in ppm, relative to the central line of a septet at δ = 39.52 ppm for deuteriodimethylsulfoxide. Infrared (IR) spectra were recorded on a NICOLET 5700 FT-IR spectrophotometer and reported in wavenumbers (cm^{-1}). Elemental analyses were obtained using a PerkinElmer Series II-2400. Mass spectra were recorded using a triple quadrupole QqQ Varian 310-MS mass spectrometer using the atmospheric-pressure ESI technique.[26] The sample solutions were infused directly into the ESI source using a programmable syringe pump at a flow rate of 1.5 mL h^{-1}. A dwell time of 14 s was used, and the spectra were accumulated for at least 5 min to increase the signal-to-noise ratio. Mass spectra were recorded in the *m/z* 100–1000 range. The experimental conditions for positive ion mode were: needle voltage 4500 V, shield 600 V, source temperature 100 °C, drying gas pressure 20 psi, nebulizing gas pressure 20 psi, detector voltage 1450 V. Tandem MS experiments were performed using argon as the collision gas (1.8 psi). The collision energy was varied from 5 to 40 V. The isotopic patterns of the measured peaks in the mass spectra were analyzed using the mMass 5.5.0 software.[27] All solvents and starting materials were purchased from commercial sources where available. Proton NMR titrations with anions were performed on a Bruker Avance 300 MHz by adding aliquots of the putative anionic guest (as the TBA salt, 0.075 M) in a solution of the receptor (0.005 M) in DMSO-d_6/0.5 % water to a solution of the receptor (0.005 M). Proton NMR titration with Zn^{2+} were performed on a Bruker Avance 300 MHz by adding aliquots of

the metal ion (as the TBA salt, 0.017 M) in a solution of the receptor (0.0025 M) in CD_3CN to a solution of the receptor (0.0025 M).

Single-crystal X-ray diffraction

Single-crystals of the ligand **L** and the ligand complexes (**1**) $[Zn(\mathbf{L})_2(MeCN)_2]^{2+}(ClO_4)_2$ 2(MeCN) and (**2**) $[Zn(\mathbf{L})_2(MeCN)_2]^{2+}(BF_4)_2$ 2(MeCN) were each selected and mounted onto a MITIGEN holders (using perfluoroether oil). Each crystal then aligned upon a Rigaku FRE+ diffractometer (equipped with HF Varimax confocal mirrors, an AFC12 goniometer, a HG Saturn 724+ detector and an Oxford Cryosystems low-temperature device (operating at T=100(2) K). The X-Ray data was then measured using profile data from ω-scans (Mo Kα radiation, Rotating Anode, 45.0 kV, 55.0 mA). The diffraction pattern of each sample, indexed with the total number of runs and images based on the strategy calculation from the program CrystalClear-SM Expert.[28] The unit cell was refined using the CrysAlisPro 1.171.41.93a software;[28] also used to perform the data reduction, data scaling and absorption corrections. The resulting structures were solved by dual methods using the ShelXT 2018/2 structure solution program,[29] refined by full matrix least squares minimization on F2 using ShelXL 2018/3[30] (within the Olex2)[31] as the graphical user interface. Basic crystallographic parameters, including bond distances and angles, torsion angles and hydrogen bonds for the three crystal structures are reported in SI Tables S1–S5.

Quantum-chemical calculations

Quantum-chemical calculations were carried out on the ligand **L** and the complex cations $[Zn(\mathbf{L})_2(MeCN)_2]^{2+}$, $[Zn(\mathbf{L})(MeCN)_2]^{2+}$, and $[Zn(\mathbf{L})(MeCN)_4]^{2+}$ at the density functional theory (DFT)[32] level with the commercial suite Gaussian 16.[33] The computational setup was validated by comparison with available structural data for **L** and the complex $[Zn(\mathbf{L})_2(MeCN)_2]^{2+}$, isolated and structurally characterized as perchlorate and tetrafluoroborate salt (see above). DFT calculations were carried out with the hybrid mPW1PW functional,[23] including a modified Perdew and Wang (PW) exchange functional coupled with the PW correlation functional.[34] Schäfer, Horn, and Ahlrichs split-valence plus polarization[24a] all-electron basis sets for light atomic species (C, H, N, O, Zn) were used in the Weigend formulation Def2SVP.[24] The geometry of all compounds was optimized (see SI, Tables S6–S10): tight SCF convergence criteria and fine numerical integration grids were used. In the case of **L**, a potential energy surface (PES) study was carried out in order to evaluate the rotational barrier around the N–C bond of the aromatic substituents (see SI, Figure S17). For all cationic complexes, generalized internal coordinates were used. A complete natural population analysis (NPA) was carried out with a Natural Bonding Orbital (NBO) (see SI, Tables S11–S14)[25] partitioning scheme in order to investigate the charge distributions.[35] The nature of the minima of each structure was verified by harmonic frequency calculations, including the determination of thermochemistry parameters [zero-point energy (ZPE) corrections and thermal corrections to enthalpy and Gibbs free energy (SI, Tables S15 and S16) and the calculation of FT-Raman frequencies. All calculations were repeated in MeCN solution, solvation being implicitly taken into account by means of the polarizable continuum model in its integral quation formalism (IEF-PCM), describing the cavity of the complexes within the reaction field (SCRF) through a set of overlapping spheres.[36] TD-DFT calculations were carried out at the optimized geometries (see SI, Figures S18–S21). Molden 6.6,[37] GaussView 6.0.16,[38] and CYLView 2.0[26] were used to analyze Kohn-Sham (KS) molecular orbital (MO) compositions and energies.

Experimental Details

Synthesis of 1-(2-aminophenyl)-3-(naphthalen-1)-yl)urea (L)

To a 50 mL DCM solution of *o*-phenylendiamine (0.64 g, 5.91 mmmol) a solution of 1-naphthylisocyanate (1.06 g, 6.29 mmol) in 20 mL of dry dichloromethane was added dropwise. The mixture was refluxed under nitrogen atmosphere for 24 hs. The progress of the reaction was monitored by TLC. After that time a precipitate was observed. Then the mixture was filtrated and the solid dried collecting the product as a crude solid.

L: Yield 95%; M.p. 203 °C; ^{1}H NMR (400 MHz, DMSO-d_6/0.5% water) δ 8.85 (s, 1H, NH), 8.16–8.21 (m, 2 H), 8.03 (d, J=8 Hz, 1H),7.92 (d, J=8 Hz, 1H),7.45–7.63 (m, 5H) 6.85 (t, J=4 Hz, 1H), 6.67 (d, J=8 Hz, 1H), 6.60 (t, J=8 Hz, 1H), 4.85(s, 2H, NH_2) ^{13}C NMR (125 MHz, DMSO-d_6) δ 153.6, 141.0, 134.8, 133.8, 128.4, 126.0, 125.6, 124.8,124.5, 123.8,122.6, 121.5, 117.0, 116.9, 116. ESI m/z 555 $[L+H]^+$. Elemental Analysis: % found (% calc. for $C_{17}H_{15}N_3O$): C 73.40 (73.63), H 5.38 (5.45), N 15.04 (15.15).

Synthesis of $[Zn(L)_2(MeCN)_2](ClO_4)_2$·2(MeCN) (1) and $[Zn(L)_2(MeCN)_2](BF_4)_2$·2(MeCN)

L and $Zn(ClO_4)_2 \cdot 6\,H_2O$ or $Zn(BF_4)_2 \cdot x\,H_2O$ were mixed in a equimolar ratio in MeCN at room temperature for 2 hs. Crystals suitable for single crystal diffraction analysis were obtained by slow diffusion of diethyl ether vapours in the resulting solutions.

(**1**) Elemental analysis % found (% calc. for $C_{42}H_{42}Cl_2N_{10}O_{10}Zn$): C 51.28 (51.31), H 4.35 (4.31), N 14.24 (14.25); ESI m/z 717 $[(Zn\mathbf{L}_2(ClO_4)]^+$;

(**2**) Elemental analysis % found (% calc. for $C_{42}H_{42}B_2F_8N_{10}O_2Zn$): C 52.58 (52.67), H 4.45 (4.42), N 14.59 (14.62); ESI m/z 705 $[(Zn\mathbf{L}_2(BF_4)]^+$

Deposition Numbers 2090222 (for **L**), 2090223 (for **1**), and 2090224 (for **2**) contain the supplementary crystallographic data for this paper. These data are provided free of charge by the joint Cambridge Crystallographic Data Centre and Fachinformationszentrum Karlsruhe Access Structures service www.ccdc.cam.ac.uk/structures.

Acknowledgements

Financial support from MIUR (PRIN 2017 project 2017EKCS35) and Università degli Studi di Cagliari (FIR 2016–2019), Fondazione di Sardegna (FdS Progetti Biennali di Ateneo, annualità 2018) is gratefully acknowledged as well as CeSAR (Centro Servizi d'Ateneo per la Ricerca) of the University of Cagliari, Italy, for ^{13}C-NMR and bidimensional NMR experiments. Dr Mark Light is gratefully acknowledged for collecting the scXRD data as is the ***EPSRC*** for the continued funding of the UK National Crystallography Service (NCS) at the University of Southampton. Open Access Funding provided by Universita degli Studi di Cagliari within the CRUI-CARE Agreement.

Conflict of Interest

The authors declare no conflict of interest.

Keywords: DFT · Fluorescence · Molecular recognition · Supramolecular chemistry · Urea

[1] F. Wöhler, *Ann. Phys.* **1828**, *87*, 253–256.
[2] C. T. Gnewuch, G. Sosnovsky, *Chem. Rev.* **1997**, *97*, 829–1014.
[3] a) N. Volz, J. Clayden, *Angew. Chem. Int. Ed.* **2011**, *50*, 12148–12155; *Angew. Chem.* **2011**, *123*, 12354–12361; b) M. Yokoya, S. Kimura, M. Yamanaka, *Chem. Eur. J.* **2021**, *27*, 5601–5614.
[4] a) J. T. Davis, P. A. Gale, R. Quesada, *Chem. Soc. Rev.* **2020**, *49*, 6056–6086; b) C. M. Dias, H. Li, H. Valkenier, L. E. Karagiannidis, P. A. Gale, D. N. Sheppard, A. P. Davis, *Org. Biomol. Chem.* **2018**, *16*, 1083–1087; c) L. A. Jowett, E. N. W. Howe, X. Wu, N. Busschaert, P. A. Gale, *Chem. Eur. J.* **2018**, *24*, 10475–10487.
[5] a) A. Casula, P. Begines, A. Bettoschi, J. G. Fernandez-Bolaños, F. Isaia, V. Lippolis, Ó. López, G. Picci, M. A. Scorciapino, C. Caltagirone, *Chem. Commun.* **2017**, *53*, 11869–11872; b) A. Casula, A. Llopis-Lorente, A. Garau, F. Isaia, M. Kubicki, V. Lippolis, F. Sancenón, R. Martínez-Máñez, A. Owczarzak, C. Santi, M. A. Scorciapino, C. Caltagirone, *Chem. Commun.* **2017**, *53*, 3729–3732; c) V. Blažek Bregović, N. Basarić, K. Mlinarić-Majerski, *Coord. Chem. Rev.* **2015**, *295*, 80–124; d) A. Casula, C. Bazzicalupi, A. Bettoschi, E. Cadoni, S. J. Coles, P. N. Horton, F. Isaia, V. Lippolis, L. K. Mapp, G. M. Marini, R. Montis, M. A. Scorciapino, C. Caltagirone, *Dalton Trans.* **2016**, *45*, 3078–3085; e) N. Kaur, G. Kaur, U. A. Fegade, A. Singh, S. K. Sahoo, A. S. Kuwar, N. Singh, *TrAC Trends Anal. Chem.* **2017**, *95*, 86–109; f) D. A. McNaughton, M. Fares, G. Picci, P. A. Gale, C. Caltagirone, *Coord. Chem. Rev.* **2021**, *427*; g) P. Yang, J. Wang, C. Jia, X.-J. Yang, B. Wu, *Eur. J. Org. Chem.* **2013**, *2013*, 3446–3454; h) Z. Yang, B. Wu, X. Huang, Y. Liu, S. Li, Y. Xia, C. Jia, X.-J. Yang, *Chem. Commun.* **2011**, *47*, 2880–2882.
[6] a) S. A. Kadam, K. Haav, L. Toom, T. Haljasorg, I. Leito, *J. Org. Chem.* **2014**, *79*, 2501–2513; b) S. A. Kadam, K. Martin, K. Haav, L. Toom, C. Mayeux, A. Pung, P. A. Gale, J. R. Hiscock, S. J. Brooks, I. L. Kirby, N. Busschaert, I. Leito, *Chem. Eur. J.* **2015**, *21*, 5145–5160.
[7] M. C. Etter, T. W. Panunto, *J. Am. Chem. Soc.* **1988**, *110*, 5896–5897.
[8] R. Bala, D. Sachdeva, M. Kumar, V. Prakash, *J. Coord. Chem.* **2020**, *73*, 2801–2837.
[9] a) L. Mazzei, M. Cianci, S. Benini, S. Ciurli, *Angew. Chem. Int. Ed.* **2019**, *58*, 7415–7419; *Angew. Chem.* **2019**, *131*, 7493–7497; b) B. Zerner, *Bioorg. Chem.* **1991**, *19*, 116–131.
[10] A. Garau, A. Bencini, A. J. Blake, C. Caltagirone, L. Conti, F. Isaia, V. Lippolis, R. Montis, P. Mariani, M. A. Scorciapino, *Dalton Trans.* **2019**, *48*, 4949–4960.
[11] a) I. Carreira-Barral, I. Fernández-Pérez, M. Mato-Iglesias, A. de Blas, C. Platas-Iglesias, D. Esteban-Gómez, *Molecules* **2018**, *23, 479*; b) I. Carreira-Barral, M. Mato-Iglesias, A. De Blas, C. Platas-Iglesias, P. A. Tasker, D. Esteban-Gómez, *Dalton Trans.* **2017**, *46*, 3192–3206; c) I. Carreira-Barral, T. Rodríguez-Blas, C. Platas-Iglesias, A. De Blas, D. Esteban-Gómez, *Inorg. Chem.* **2014**, *53*, 2554–2568.
[12] R. Montis, A. Bencini, S. J. Coles, L. Conti, L. Fusaro, P. A. Gale, C. Giorgi, P. N. Horton, V. Lippolis, L. K. Mapp, C. Caltagirone, *Chem. Commun.* **2019**, *55*, 2745–2748.
[13] a) V. Amendola, M. Boiocchi, L. Fabbrizzi, A. Palchetti, *Chem. Eur. J.* **2005**, *11*, 120–127; b) S. Camiolo, P. A. Gale, M. B. Hursthouse, M. E. Light, A. J. Shi, *Chem. Commun.* **2002**, 758–759; c) L. S. Evans, P. A. Gale, M. E. Light, R. Quesada, *Chem. Commun.* **2006**, 965–967; d) T. Gunnlaugsson, P. E. Kruger, P. Jensen, F. M. Pfeffer, G. M. Hussey, *Tetrahedron Lett.* **2003**, *44*, 8909–8913.
[14] J. T. Mague, S. K. Mohamed, M. Akkurt, O. A. Omran, M. R. Albayati, *Acta Crystallogr. Sect. E* **2015**, *71*, o88-o89.
[15] a) A. Casula, M. Fornasier, R. Montis, A. Bettoschi, S. P. Argent, A. J. Blake, V. Lippolis, L. Marongiu, G. Picci, J. P. Tidey, C. Caltagirone, *Supramol. Chem.* **2017**, *29*, 875–886; b) R. Custelcean, *Chem. Commun.* **2008**, 295–307; c) M. Olivari, R. Montis, L. E. Karagiannidis, P. N. Horton, L. K. Mapp, S. J. Coles, M. E. Light, P. A. Gale, C. Caltagirone, *Dalton Trans.* **2015**, *44*, 2138–2149; d) L. S. Reddy, S. K. Chandran, S. George, N. J. Babu, A. Nangia, *Cryst. Growth Des.* **2007**, *7*, 2675–2690.
[16] a) D. Brynn Hibbert, P. Thordarson, *Chem. Commun.* **2016**, *52*, 12792–12805; b) P. Thordarson, *Chem. Soc. Rev.* **2011**, *40*, 1305–1323.
[17] L. Pfeifer, K. M. Engle, G. W. Pidgeon, H. A. Sparkes, A. L. Thompson, J. M. Brown, V. Gouverneur, *J. Am. Chem. Soc.* **2016**, *138*, 13314–13325.
[18] a) L. Drakopoulou, C. P. Raptopoulou, A. Terzis, G. S. Papaefstathiou, *Bioinorg. Chem. Appl.* **2010**, *2010*, 618202; b) R. Keuleers, H. O. Desseyn, G. S. Papaefstathiou, L. Drakopoulou, S. P. Perlepes, C. P. Raptopoulou, A. Terzis, *Trans. Metal Chem.* **2003**, *28*, 548–557.
[19] a) P. S. Gentile, P. Carfagno, S. Haddad, L. Campisi, *Inorg. Chim. Acta* **1972**, *6*, 296–298; b) D. S. Sagatys, R. C. Bott, G. Smith, K. A. Byriel, C. H. L. Kennard, *Polyhedron* **1992**, *11*, 49–52.
[20] a) A. Karmakar, B. Manna, A. V. Desai, B. Joarder, S. K. Ghosh, *Inorg. Chem.* **2014**, *53*, 12225–12227; b) W. C. Tong, J. C. Liu, Q. Y. Wang, L. Yang, T. L. Zhang, *Z. Anorg. Allg. Chem.* **2014**, *640*, 2991–2997; c) L. Yang, W. Tong, H. Li, G. Zhang, J. Liu, *Inorg. Chim. Acta* **2017**, *466*, 405–409; d) J. Zhang, T. Zhang, J. Zhang, L. Yang, Y. Cui, X. Hu, Z. Liu, *Struct. Chem.* **2008**, *19*, 321–328.
[21] a) N. N. Adarsh, D. K. Kumar, P. Dastidar, *CrystEngComm* **2008**, *10*, 1565–1573; b) R. Custelcean, B. A. Moyer, V. S. Bryantsev, B. P. Hay, *Cryst. Growth Des.* **2006**, *6*, 555–563; c) D. R. Turner, M. Henry, C. Wilkinson, G. J. McIntyre, S. A. Mason, A. E. Goeta, J. W. Steed, *J. Am. Chem. Soc.* **2005**, *127*, 11063–11074; d) D. R. Turner, M. B. Hursthouse, M. E. Light, J. W. Steed, *Chem. Commun.* **2004**, 1354–1355; e) B. Wu, J. Liang, Y. Zhao, M. Li, S. Li, Y. Liu, Y. Zhang, X.-J. Yang, *CrystEngComm* **2010**, *12*, 2129–2134.
[22] C. Adamo, V. Barone, *J. Chem. Phys.* **1998**, *108*, 664–675.
[23] a) A. Schäfer, H. Horn, R. Ahlrichs, *J. Chem. Phys.* **1992**, *97*, 2571–2577; b) F. Weigend, R. Ahlrichs, *Phys. Chem. Chem. Phys.* **2005**, *7*, 3297–3305.
[24] A. E. Reed, R. B. Weinstock, F. Weinhold, *J. Chem. Phys.* **1985**, *83*, 735–746.
[25] E. Cadoni, E. Valletta, G. Caddeo, F. Isaia, M. G. Cabiddu, S. Vascellari, T. Pivetta, *J. Inorg. Biochem.* **2017**, *173*, 126–133.
[26] M. Strohalm, D. Kavan, P. Novák, M. Volný, V. Havlíček, *Anal. Chem.* **2010**, *82*, 4648–4651.
[27] a) Rigaku, V2.0 r7 **2011**; b) Rigaku Oxford Diffraction, 2020.
[28] G. Sheldrick, *Acta Crystallogr. Sect. A* **2015**, *71*, 3–8.
[29] G. Sheldrick, *Acta Crystallogr. Sect. C* **2015**, *71*, 3–8.
[30] O. V. Dolomanov, L. J. Bourhis, R. J. Gildea, J. A. K. Howard, H. Puschmann, *J. Appl. Crystallogr.* **2009**, *42*, 339–341.
[31] W. Koch,M. C. Hothausen, *A Chemist's Guide to Density Functional Theory, 2nd Edition*, **2002**.
[32] M. J. Frisch, H. B. Schlegel, G. E. Scuseria, M. A. Robb, J. R. Cheeseman, G. Scalmani, V. Barone, G. A. Petersson, H. Nakatsuji, X. Li, M. Caricato, A. V. Marenich, J. Bloino, B. G. Janesko, R. Gomperts, B. Mennucci, H. P. Hratchian, J. V. Ortiz, A. F. Izmaylov, J. L. Sonnenberg, D. Williams-Young, F. Ding, F. Lipparini, F. Egidi, J. Goings, B. Peng, A. Petrone, T. Henderson, D. Ranasinghe, V. G. Zakrzewski, J. Gao, N. Rega, G. Zheng, W. Liang, M. Hada, M. Ehara, K. Toyota, R. Fukuda, J. Hasegawa, M. Ishida, T. Nakajima, Y. Honda, O. Kitao, H. Nakai, T. Vreven, K. Throssell, J. A. Montgomery, Jr., J. E. Peralta, F. Ogliaro, M. J. Bearpark, J. J. Heyd, E. N. Brothers, K. N. Kudin, V. N. Staroverov, T. A. Keith, R. Kobayashi, J. Normand, K. Raghavachari, A. P. Rendell, J. C. Burant, S. S. Iyengar, J. Tomasi, M. Cossi, J. M. Millam, M. Klene, C. Adamo, R. Cammi, J. W. Ochterski, R. L. Martin, K. Morokuma, O. Farkas, J. B. Foresman, D. J. Fox, Gaussian, Inc., Wallingford CT, **2016**.
[33] a) J. P. Perdew, J. A. Chevary, S. H. Vosko, K. A. Jackson, M. R. Pederson, D. J. Singh, C. Fiolhais, *Phys. Rev. B* **1992**, *46*, 6671–6687; b) J. P. Perdew, J. A. Chevary, S. H. Vosko, K. A. Jackson, M. R. Pederson, D. J. Singh, C. Fiolhais, *Phys. Rev. B* **1993**, *48*, 4978.
[34] K. B. Wiberg, *Tetrahedron* **1968**, *24*, 1083–1096.
[35] J. Tomasi, B. Mennucci, R. Cammi, *Chem. Rev.* **2005**, *105*, 2999–3094.
[36] G. Schaftenaar, J. H. Noordik, *J. Comp.-Aided Mol. Des.* **2000**, *14*, 123–134.
[37] R. Dennington, T. Keith, J.Millam, (2009) Gauss View, Version 5. Semichem Inc., Shawnee Mission.
[38] L. Skripnikov, Chemissian Version 4.67, Visualization Computer Program, **2020**, http://www.chemissian.com.

Manuscript received: July 7, 2021
Revised manuscript received: August 13, 2021
Accepted manuscript online: August 17, 2021